IEEE Access
Multidisciplinary | Rapid Review | Open Access Journal

Date of publication xxxx 00, 0000, date of current version xxxx 00, 0000.

Digital Object Identifier 10.1109/ACCESS.2024.0429000

Carrier-Based PWM Strategy for Output Current Ripple Minimization in Multiphase Motor Drives

ANTONIO FEMIA[1], (Student Member, IEEE), RICCARDO A. TESTA[1,2], MICHELE MENGONI[1], (Member, IEEE), GABRIELE RIZZOLI[1], LUCA VANCINI[1], (Member, IEEE), LUCA ZARRI[1], (Senior Member, IEEE), AND ANGELO TANI[1]

[1]University of Bologna, Bologna, CO 40136 IT
[2]Ocem Power Electronics, Valsamoggia (BO), CO 40056 IT

Corresponding author: Luca Zarri (e-mail: luca.zarri2@unibo.it).

This work was supported in part by the National Recovery and Resilience Plan (NRRP), Mission 4 Component 2 Investment 1.3 - Call for tender No. 1561 of 11.10.2022 of Ministero dell'Università e della Ricerca (MUR), funded by the European Union – NextGenerationEU. Award Number: Project code PE0000021, Concession Decree No. 1561 of 11.10.2022 adopted by Ministero dell'Università e della Ricerca (MUR), CUP "J33C22002890007". Project title "Network 4 Energy Sustainable Transition – NEST".

ABSTRACT Recently, multiphase drives have emerged as a notable alternative for three-phase drives in several domains, including electric marine propulsion, locomotive traction, and high-power industrial applications where fault tolerance and high reliability are required. This study uses a graphical approach to develop a new carrier-based Pulse-Width Modulation (PWM) that reduces the root-mean-square value of the output current ripple in two-level multiphase inverters with an odd number of phases. The optimization process calculates the optimal common-mode voltage for each switching period. Numerical models and experiments with five- and seven-phase inverters demonstrate the effectiveness of the developed PWM technique, which can reduce the number of commutations while obtaining the lowest output current ripple.

INDEX TERMS Multiphase Drives, Multiphase Machines, Voltage Sources Inverters (VSI), Pulse Width Modulation (PWM), Current Ripple, Modulation Strategies, Current Quality, Current Ripple Minimization.

I. INTRODUCTION

Multiphase drives are an intriguing technology that splits electric power between more than three phases and is ideal for high-power applications [1], [2]. Compared to traditional three-phase drives, with equal power, multiphase motor drives have several advantages. The current is distributed across several phases, allowing for lower-rated power switches and enabling higher inverter ratings without changing the technology of the switches [3]. An increased number of phases correlates to a higher number of degrees of freedom, which can be efficiently employed to enhance the fault tolerance or torque density of the drive [4]. If an open-phase fault occurs, fault-tolerant control strategies can be adopted, allowing the machine to continue operating with the remaining healthy phases, albeit with lower performance. The extra degrees of freedom can be utilized to enhance the torque density by adding spatial harmonics to the magnetic field of the electric machines. Typically, the maximum value of the magnetic field in the air gap of an electrical machine is selected to prevent excessive magnetic saturation. In a multiphase drive, the air gap field can be broken down into harmonic components that can be individually controlled. These harmonics, with appropriate amplitudes, can be synchronized so that their peak values are out of sync with the fundamental one. Consequently, the amplitude of the fundamental component can be increased without altering the peak value of the overall field wave, thereby boosting the torque.

However, the complexity of the control design increases, and establishing appropriate and adaptable control strategies for N-phase Voltage Source Inverters (VSIs) is crucial to exploit the strengths of N-phase motor drives. Table 1 presents a chronological listing of the most pertinent research papers addressing the issue of modulation strategies for multiphase electric drives. This provides a clear understanding of the evolution of research in this field over the past 15 years. As can be seen, two modulation techniques, Space-Vector Modulation (SVM) and carrier-based Pulse-Width Modulation (PWM), have been developed, but they have been demonstrated to be inherently equivalent [5], [6]. Currently, PWM is often preferred owing to its simplicity. Over the years, various efforts

TABLE 1. Most relevant journal research papers that address the problem of modulation for multiphase inverters.

Year	Ref.	Topic	Topology	Modulation strategy
1985	[23]	Optimal PWM strategy for the minimum RMS value of the load current ripple	Three-phase inverters	Carrier-Based PWM
2008	[32]	General PWM strategy and modulation boundaries for 7-phase inverters	7-phase inverters	Carrier-based PWM
2008	[33]	General modulation boundaries for multiphase inverters	Inverters with an odd number of phases	Carrier-based PWM
2009	[5]	Complete theory of space vector modulation for multiphase inverters	Inverters with an odd number of phases	SVM
2009	[24]	Survey paper. Comparison of different modulation strategies in terms of current ripple	5-phase inverters	Carrier-Based PWM
2010	[25]	Survey paper. Comparison of different modulation strategies in terms of current ripple	Inverters with an odd number of phases	Carrier-Based PWM
2010	[9]	Carrier-based PWM strategy to minimize the switching losses of multiphase inverters	Inverters with an odd number of phases	Carrier-Based PWM
2011	[26]	Survey paper. Comparison of different modulation strategies in terms of flux ripple	Inverters with an odd number of phases	SVM
2011	[27]	Survey paper. Comparison of different modulation strategies in terms of current ripple	Inverters with an odd number of phases	SVM
2011	[28]	Optimal carrier-based PWM strategy for the minimum RMS value of the current ripple	5-phase inverters	Carrier-Based PWM
2013	[29]	Comparison of modulation strategy in terms of peak-to-peak value of the current ripple	5-phase inverters	Carrier-Based PWM
2015	[30]	Carrier-based PWM strategy for the current ripple reduction	6-phase inverters with symmetrical machines	Carrier-Based PWM
2020	[6]	SVM strategies and their equivalent carrier-based PWM strategies for multilevel-multiphase inverters	Multilevel-multiphase inverters with 5,6,7 phases	SVM, Carrier-Based PWM
2021	[21]	Selective harmonic elimination for torque ripple reduction	Dual-three-phase inverters	Carrier-Based PWM
2021	[10]	Overmodulation strategies for five-phase inverters	5-phase inverters	Carrier-Based PWM
2022	[11]	Adaptive overmodulation strategies for five-phase inverters	5-phase inverters	Carrier-Based PWM
2022	[18]	Optimized PWM modulation to improve the current quality	Dual-three-phase inverters	Carrier-Based PWM
2022	[7]	Enhanced PWM strategy to reduce the load common-mode voltage	Inverters with an odd number of phases	SVM
2023	[8]	Carrier-based PWM strategy to reduce the common-mode voltage	Multilevel-multiphase inverters with n phases	Carrier-Based PWM
2023	[31]	Optimal carrier-based PWM strategy for the current ripple reduction	6-phase inverters with asymmetrical machines	Carrier-Based PWM
2024	[19]	Survey paper. Comparison of PWM modulation to improve the current quality	Dual-three-phase inverters	Carrier-Based PWM and SVM

have been made to enhance the performance of multiphase drives in terms of efficiency, quality of output voltages and input currents, common-mode disturbances, operating range, and flexibility [7]–[11]. A recurring topic related to power converters is the output current quality.

A reduction in the switching ripple of the phase currents has a visible impact on the electric drive. The transition from a sinusoidal AC supply to a PWM supply may increase the losses within the magnetic circuit of electric machines by more than 15% because the current and voltage waveform can be significantly distorted in comparison to the sinusoidal form [12]. This distortion causes relatively small loops adjacent to the main hysteresis loop [13]. The utilization of permanent magnets on the rotor surface confers design advantages, as it enables the creation of a robust magnetic field in electrical machines. However, they are susceptible to eddy current losses caused by the field harmonics due to the PWM supply. The eddy current losses are more significant than hysteresis losses in practical electrical machine applications. Since the supply frequencies are increasing, facilitated by new SiC or GaN power transistors, the minor hysteresis loops are significantly influenced by the skin effect, which makes the theoretical modelling of the losses challenging [14], [15]. The flux density variations in electrical machines caused by PWM are typically only a few milliTesla. PWM iron loss is the dominant loss component at high switching frequency. Discontinuous modulation strategies result in higher machine PWM losses due to larger current harmonics, but these losses decrease as the switching frequency rises [16].

In high-power applications, low-carrier-ratio operation is needed to reduce switching losses and meet thermal constraints [17]. However, the limited switching frequency results in increased stator current harmonics and torque pulsation. There are two primary research directions for mitigating torque pulsation with low-carrier-ratio operations. The first category involves mitigating torque ripple by adjusting the modulation strategy online. This result can be achieved by reducing the harmonic content of the torque-producing currents using modified PWM switching patterns. For instance, optimized PWM strategies have been proposed to reduce the current harmonics for dual three-phase PMSM [18], [19]. Another approach involves modifying the modulation strategy directly to reduce the torque ripple instead of the current ripple [20]. The second category of methods for torque ripple mitigation involves offline optimization of the PWM strategy, for example, through selective torque harmonic elimination [21]. Furthermore, in machines built for high-speed operations and with low DC-link voltage, the per-unit reactance is usually very low. This can lead to significant current and torque ripple, particularly when the machine is powered by a PWM inverter with a low switching frequency. The torque ripples may cause speed oscillation and create strong vibrations and noises that can be damaging to both the mechanical system and people nearby [22].

Since the development of the first three-phase inverters, ripple reduction has been a major concern. It has been proven that injecting a common-mode third harmonic voltage with an amplitude equivalent to $1/4$ of the fundamental voltage minimizes the Root Mean Square (RMS) value of the output current ripple [23]. In the initial research on multiphase inverters, an SVM technique was developed for 5-phase inverters [24]. The analysis was aimed at calculating the RMS value of the harmonic flux rather than the current ripple to avoid dependence on the load inductances, which may differ

in each vector space of a multiphase machine. Despite some specific assumptions, it was demonstrated that voltages acting in harmonic subspaces other than the fundamental one may significantly impact the output current ripple. The injection of a common-mode harmonic voltage is not effective, in contrast to three-phase systems, where adding suitable odd-order harmonic components to the common-mode voltage improves the output switching ripple and increases the dc-bus utilization in comparison to Sinusoidal PWM (SPWM). A subsequent study, based on the so-called polygonal approach, which analyzes the $(N–1)/2$ polygon configurations of an N-phase system (N is an odd number), provided new confirmation. This approach was developed to simplify the calculation of the RMS value of the current ripple [25].

Among the available modulation strategies, the SVM was initially the most investigated [26], [27]. Several techniques were compared, and the issue of identifying the most performing was raised. For five-phase inverters, the common-mode voltage that minimizes the RMS value of the output current ripple in a switching period is ultimately determined as a function of the reference voltage vectors in subspaces $\alpha_1-\beta_1$ and $\alpha_3-\beta_3$ [28]. This result was obtained through complex analytical calculations and demonstrated that SPWM is the optimal strategy when only one reference space vector is different from zero. An alternative approach to the analysis of the switching ripple in five-phase inverters was based on the estimation of the peak-to-peak amplitude of the current ripple, derived as a function of the modulation index under sinusoidal operating conditions [29]. Subsequent research focused on different structures of multiphase drives, such as symmetrical and asymmetrical six-phase topologies [30], [31].

This work focuses on the modulation strategy with the minimum RMS value of the output current switching ripple for multiphase inverters with an odd number of phases. Compared to previous studies, this paper provides the following contributions:

- An analytical model is developed, which leads to a closed-form expression of the zero-sequence component of the modulating signals that theoretically minimizes the RMS value of the load current ripple.
- The optimization is applied in each switching period and is based on the Vector Space Decomposition (VSD). Consequently, the aforementioned optimization is not limited to sinusoidal signals or steady-state operating conditions.
- The proposed strategy reduces the number of commutations of the power switches compared with the most common strategies for high modulation index values.
- The analysis finds again the optimal strategies developed for three- and five-phase machines. Furthermore, it confirms that SPWM offers the optimal quality of the output current for any odd number of phases greater than three if only one reference voltage vector is different from zero.

Motors with an odd number of phases (e.g., 3, 5, 7, 9) have the highest degree of symmetry. Nevertheless, the most investigated multiphase motors have a number of phases that is a multiple of three (e.g., 6 or 9) because they can be designed as three-phase modules operating together. However, the electrical behavior of a multi-three-phase motor is determined by the way the various three-phase windings are connected, i.e., whether they are connected to one or distinct neutral points. Therefore, since multi-three-phase topology is not unique, the method described in the paper focuses only on machines with an odd number of phases (3, 5, 7, 9, …) under the assumption that they are all connected to a single star point.

The remainder of this paper is organized as follows. The mathematical model is presented in Section II. Section III shows the simulation results and highlights the outcomes of the investigation. Section IV illustrates the experimental results obtained by means of two induction machines with five and seven phases, respectively. Finally, Section V summarizes the most important findings.

II. ANALYSIS OF THE OUTPUT CURRENT RIPPLE

A. FUNDAMENTALS OF CARRIER-BASED PWM FOR MULTIPHASE INVERTERS

A schematic of a multiphase inverter is shown in Fig. 1. In multiphase systems, the concepts of space vectors and zero-sequence components are frequently employed. Given an odd set of N real quantities $x_1, x_2, \ldots, x_N$, the following linear transformations define a new set of variables:

$$\begin{aligned} x_0 &= \frac{1}{N}\sum_{k=1}^{N} x_k \\ \bar{x}_\rho &= \frac{2}{N}\sum_{k=1}^{N} x_k \bar{\alpha}_k^\rho \quad \rho = 1,3,...,N-2 \end{aligned} \tag{1}$$

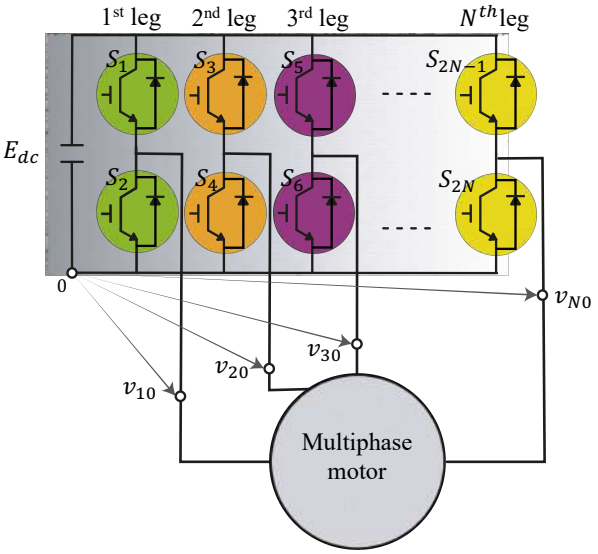

FIGURE 1. Multiphase inverter supplying a multiphase machine.

where

$$\bar{\alpha}_k = e^{j\frac{2\pi}{N}(k-1)}. \tag{2}$$

The real quantity x_0 is the zero-sequence component, whereas $\bar{x}_1, \bar{x}_3, ..., \bar{x}_{N-2}$ are complex quantities called "space vectors." If $m_1, m_2, ..., m_N$ are the command signals of the inverter legs, with values of 0 or 1, and E_{dc} is the dc-link voltage, the instantaneous output voltage vectors are as follows:

$$\bar{v}_\rho = \frac{2}{N} E_{dc} \sum_{k=1}^{N} m_k \bar{\alpha}_k^\rho \quad \rho = 1, 3, ..., N-2. \tag{3}$$

Given the desired average voltage vectors $\bar{v}_{1,ref}, \bar{v}_{3,ref}, ..., \bar{v}_{N-2,ref}$ over a switching period, solving the modulation problem of a multiphase inverter requires finding the N command signals of the inverter legs. According to the principles of PWM, the command signals can be generated by comparing N modulating signals $m_{1,ref}, m_{2,ref}, ..., m_{N,ref}$ with a triangular carrier. The k-th modulating signal $m_{k,ref}$ can be calculated by inverting (1):

$$\begin{aligned} m_{k,ref} &= m_{0,ref} + n_{k,ref} \\ n_{k,ref} &= \frac{1}{E_{dc}} \sum_{k=1}^{N-2} \bar{v}_{\rho,ref} \cdot \bar{\alpha}_k^\rho \quad k = 1, 2, ..., N \end{aligned} \tag{4}$$

where "$\cdot$" is the dot operator, defined as the real part of the product of the first operand multiplied by the complex conjugate of the second operand, and $m_{0,ref}$ is the zero-sequence component of the modulating signals.

The zero-sequence component $m_{0,ref}$ is a degree of freedom that can be chosen to improve the PWM performance. To prevent overmodulation, the modulating signals must remain within the following range:

$$m_{k,ref} \in [0, 1] \quad k = 1, 2, ..., N. \tag{5}$$

Tab. 2 lists some noteworthy values of $m_{0,ref}$, which correspond to well-known modulation strategies for multiphase inverters. In Tab. 2, the quantity $\bar{m}_{\rho,ref}$ is defined as the ratio of $\bar{v}_{\rho,ref}$ and E_{dc}.

Constraints (5) result in lower and upper limits for the magnitude of the modulating signals, which define the output voltage range of the converter [32], [33].

As can be seen in (4), the modulation process for multiphase inverters is similar to that for three-phase inverters,

TABLE 2. Value of $m_{0,ref}$ for different PWM modulation strategies.

Name	$m_{0,ref}$
Sinusoidal (S)	$m_{0,S} = \frac{1}{2}$
Discontinuous (DMIN)	$m_{0,DMIN} = -\min_{k=1,...,N}\left(\sum_\rho \bar{m}_{\rho,ref} \cdot \bar{\alpha}_k^\rho\right)$
Discontinuous (DMAX)	$m_{0,DMAX} = 1 - \max_{k=1,...,N}\left(\sum_\rho \bar{m}_{\rho,ref} \cdot \bar{\alpha}_k^\rho\right)$
Space Vector (SVPWM)	$m_{0,SV} = \frac{1}{2}(m_{0,DMIN} + m_{0,DMAX})$

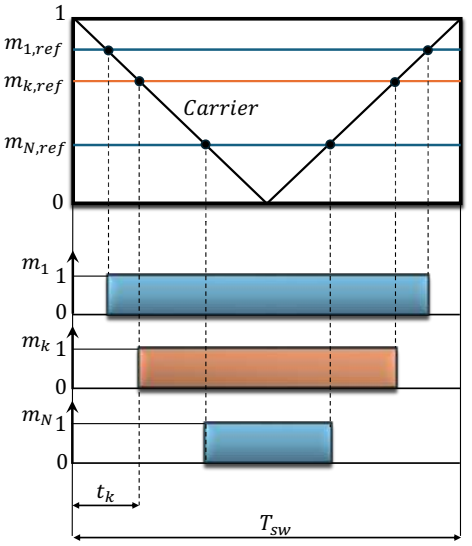

FIGURE 2. Generation of the switching signals in a *N*-phase inverter according to the carrier-based PWM.

i.e., the modulating signals are compared with the carrier signal to generate the gate control signals over the switching period T_{sw}, as shown in Fig. 2. However, the calculation of the modulating signals may be more complex, as it depends on the reference voltage vectors in all subspaces according to the vector space decomposition. If the reference voltage vectors in the harmonic subspaces are zero, the control system complexity does not change significantly. On the other hand, if the control system aims to manage the extra spatial harmonic components of the magnetic field, the calculation of the reference voltage vectors may become challenging, depending on the specific feature that the control system is targeting, such as high-torque density, fault-tolerant operation, and online parameter estimation.

B. MODULATION STRATEGY WITH MINIMUM RMS VALUE OF THE OUTPUT CURRENT RIPPLE

The output current vectors $\bar{i}_1, \bar{i}_3, ..., \bar{i}_{N-2}$ deviate from their desired trajectories owing to the discrepancy between the actual voltage vectors $\bar{v}_1(t), \bar{v}_3(t), ..., \bar{v}_{N-2}(t)$ and the desired values $\bar{v}_{1,ref}, \bar{v}_{3,ref}, ..., \bar{v}_{N-2,ref}$. However, the switching pattern of the actual voltage vectors is arranged to match the desired average values over the switching period.

The deviation $\Delta\bar{i}_\rho$ of each current vector from its average value over a switching period T_{sw} is governed by the following approximated differential equation, which neglects the effect of the load resistance in high-frequency transients:

$$L_\rho \frac{d\Delta\bar{i}_\rho}{dt} = \bar{v}_\rho - \bar{v}_{\rho,ref} \tag{6}$$

where $\bar{v}_\rho$ and L_ρ ($\rho = 1, 3, ..., N-2$) are the actual voltage space vector and the high-frequency equivalent load inductance in subspace ρ. The average deviations of the currents

and voltages from their desired values can be assumed zero over T_{sw}, so the following constraints are satisfied:

$$\int_0^{T_{sw}} \Delta\bar{i}_\rho \, dt = 0 \tag{7}$$

$$\int_0^{T_{sw}} (\bar{v}_\rho - \bar{v}_{ref,\rho}) \, dt = 0. \tag{8}$$

It is assumed that the modulation strategy generates a symmetric switching pattern with respect to the midpoint of the switching period. This property implies that the sequence of transitions from one inverter configuration to the next in the first half period is repeated backward in the second half. Fig. 3 shows an example of the trajectory of the current ripple over a switching period for a five-phase inverter. The deviation $\Delta\bar{i}_\rho$ is zero at $t = 0$, $t = T_{sw}/2$, and $t = T_{sw}$. Each color vector corresponds to a specific inverter configuration. The trajectory of $\Delta\bar{i}_\rho$ is symmetric with respect to the origin of the reference frame, so the analysis of the current ripple can be limited to half of the switching period, T (i.e., $T = \frac{T_{sw}}{2}$).

Furthermore, the current ripple $\Delta\bar{i}_\rho$ can be expressed as the sum of its average value $\bar{i}^0_{rip,0}$ over the half period T and the zero-mean deviation $\bar{i}_{rip}$, as stated below:

$$\Delta\bar{i}_\rho = \bar{i}^0_{rip,\rho} + \bar{i}_{rip,\rho} \tag{9}$$

$$\bar{i}^0_{rip,\rho} = \frac{1}{T}\int_0^T \Delta\bar{i}_\rho dt. \tag{10}$$

The total RMS value of the current ripple, extended to all phases and over a switching period T_{sw}, is as follows:

$$T_{sw}\Delta I^2_{RMS} = \sum_{k=1}^{N}\int_0^{T_{sw}} \Delta i_k^2 dt = \frac{N}{2}\sum_{\rho=1,3,\ldots}^{N-2}\int_0^{T_{sw}} |\Delta\bar{i}_\rho|^2 dt \tag{11}$$

where Δi_k is the deviation in the k-th load current. Due to the symmetric trajectory of the current ripple, the integrals in (11) can be rewritten as integrals over a half period. In addition, by combining (9) and (11), the following result can be obtained:

$$T_{sw}\Delta I^2_{RMS} = N\sum_{\rho=1,3,\ldots}^{N-2}\left(T|\bar{i}^0_{rip,\rho}|^2 + \int_0^T |\bar{i}_{rip,\rho}|^2 dt\right). \tag{12}$$

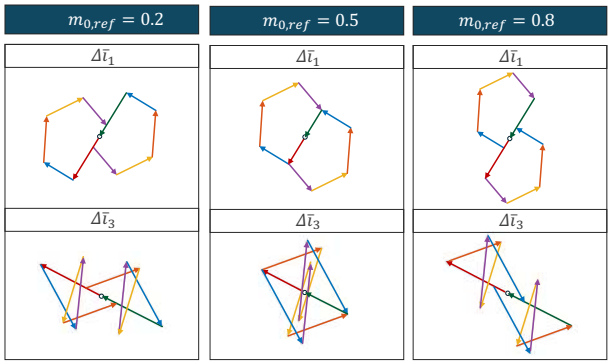

FIGURE 3. Deviation of the current space vectors of a five-phase inverter from their ideal trajectories in subspaces 1 and 3 over a switching period for different values of $m_{0,ref}$.

It can be demonstrated that the quantity $\int_0^T |\bar{i}_{rip,\rho}|^2 dt$, which appears in (12), is constant and independent of $m_{0,ref}$, similar to the calculation of the center of mass of a plane curve. This result can be readily understood by examining Fig. 3, which shows the trajectories of $\Delta\bar{i}_1$ and $\Delta\bar{i}_3$ over a switching period for three increasing values of $m_{0,ref}$ in a five-phase inverter. As can be seen, each curve is composed of two parts, symmetrically disposed with respect to the origin, which rigidly translate without changing their shape as long as $m_{0,ref}$ increases. Consequently, to reduce the RMS value of the current ripple, it is necessary to minimize the quantity $\sum_{\rho=1,3,\ldots}^{N-2} |\bar{i}^0_{rip,\rho}|^2$, the only one sensitive to $m_{0,ref}$ in (12).

The derivative of (12) with respect to $m_{0,ref}$ is expressed as follows:

$$\frac{d(T_{sw}\Delta I^2_{RMS})}{dm_{0,ref}} = NT\sum_{\rho=1,3,\ldots}^{N-2} 2\bar{i}^0_{rip,\rho}\cdot\frac{d\bar{i}^0_{rip,\rho}}{dm_{0,ref}}. \tag{13}$$

To evaluate (13) and find the expression of $\bar{i}^0_{rip,\rho}$, two steps are necessary. The initial step is to determine $\Delta\bar{i}_\rho$ by integrating (6).

$$\Delta\bar{i}_\rho(t) = \frac{1}{L_\rho}\int_0^t \Big(\bar{v}_\rho(\tau) - \bar{v}_{\rho,ref}\Big) d\tau. \tag{14}$$

Then, combining (14), (10) and (3) yields the following expression for $\bar{i}^0_{rip,\rho}$:

$$\bar{i}^0_{rip,\rho} = \frac{1}{T}\frac{2}{N}\frac{E_{dc}}{L_\rho}\sum_{k=1}^{N}\left[\int_0^T\left(\int_0^t m_k\bar{\alpha}^\rho_k d\tau\right)dt\right] - \frac{T}{2}\frac{\bar{v}_{\rho,ref}}{L_\rho}. \tag{15}$$

Equation (15) can be simplified by noting from Fig. 2 that the following equality holds:

$$\int_0^t m_k d\tau = \begin{cases} 0 & if \quad t < t_k \\ t - t_k & otherwise \end{cases} \tag{16}$$

where t_k is the transition time of m_k from 0 to 1.

Substituting (16) into (15) gives the following result:

$$\bar{i}^0_{rip,\rho} = \frac{T}{2L_\rho}\left[\frac{2}{N}E_{dc}\sum_{k=1}^{N}\left(1 - \frac{t_k}{T}\right)^2\bar{\alpha}^\rho_k - \bar{v}_{\rho,ref}\right]. \tag{17}$$

Fig. 2 shows that the quantity $1 - \frac{t_k}{T}$ is equal to $m_{k,ref}$, so (17) can be rewritten in a more compact form:

$$\bar{i}^0_{rip,\rho} = \frac{T}{2L_\rho}\left[\frac{2}{N}E_{dc}\sum_{k=1}^{N} m^2_{k,ref}\bar{\alpha}^\rho_k - \bar{v}_{\rho,ref}\right]. \tag{18}$$

The leg modulating signals can be expressed as functions of the zero-sequence component $m_{0,ref}$ through (4). Consequently, (18) becomes as follows:

$$\bar{i}^0_{rip,\rho} = \frac{T}{2L_\rho}\left[\frac{2}{N}E_{dc}\sum_{k=1}^{N} n^2_{k,ref}\bar{\alpha}^\rho_k + (2m_{0,ref} - 1)\bar{v}_{ref,\rho}\right]. \tag{19}$$

After some calculations, (13) turns out to be a linear function of $m_{0,ref}$:

$$\frac{d(T_{sw}\Delta I^2_{RMS})}{dm_{0,ref}} = A(2m_{0,ref} - 1) + B \tag{20}$$

where

$$A = 2NT^2 \sum_{\rho=1,3,\dots}^{N-2} \frac{|\bar{v}_{\rho,ref}|^2}{L_\rho^2}$$
$$B = 2NT^2 \sum_{\rho=1,3,\dots}^{N-2} \left(\frac{2}{N} \frac{E_{dc}}{L_\rho^2} \sum_{k=1}^{N} n_{k,ref}^2 \bar{\alpha}_k^\rho \cdot \bar{v}_{\rho,ref} \right). \tag{21}$$

To find the value of $m_{0,ref}$ corresponding to the minimum ripple, the derivative must be set equal to zero:

$$m_{0,OPT} = \frac{1}{2} \left(1 - \frac{\sum_{\rho=1,3,\dots}^{N-2} \frac{2}{N} \sum_{k=1}^{N} n_{k,ref}^2 \bar{\alpha}_k^\rho \cdot \frac{\bar{m}_{\rho,ref}}{L_\rho^2}}{\sum_{\rho=1,3,\dots}^{N-2} \frac{|\bar{m}_{\rho,ref}|^2}{L_\rho^2}} \right). \tag{22}$$

The value of $m_{0,OPT}$ resulting from (22) corresponds to a minimum of the current ripple because the second derivative, obtained by deriving (20) once again, equals A, which is positive.

The value of $m_{0,OPT}$ in (22) is valid if the resulting modulating signals satisfy the constraints (5); otherwise, $m_{0,OPT}$ must be constrained between $m_{0,DMIN}$ and $m_{0,DMAX}$.

Equation (22) is written in a mixed form, i.e., it combines the dimensionless reference voltage vectors $\bar{m}_{1,ref}, \bar{m}_{3,ref}, \dots, \bar{m}_{N-2,ref}$, sometimes called duty-cycle space vectors, and the scalar signals $n_{1,ref}, n_{2,ref}, \dots, n_{N,ref}$. The expressions of (22) as functions of the signals $n_{1,ref}, n_{2,ref}, \dots, n_{N,ref}$ or the dimensionless voltage vectors $\bar{m}_{1,ref}, \bar{m}_{3,ref}, \dots, \bar{m}_{N-2,ref}$ are derived in the next sections.

C. EXPRESSION OF $m_{0,opt}$ AS A FUNCTION OF THE MODULATING SIGNALS

Let us define the new variables $l_1, l_2, \dots, l_N$ as follows:

$$l_k = \sum_{\rho=1,3,\dots}^{N-2} \frac{\bar{m}_{\rho,ref}}{L_\rho^2} \cdot \bar{\alpha}_k^\rho. \tag{23}$$

Then, (22) can be written as follows:

$$m_{0,OPT} = \frac{1}{2} \left(1 - \frac{\sum_{k=1}^{N} n_{k,ref}^2 l_k}{\sum_{k=1}^{N} n_{k,ref} l_k} \right). \tag{24}$$

If all inductances are equal to the same value L, then l_k is equal to $n_{k,ref}/L^2$ for any k, and (24) takes a simpler form:

$$m_{0,OPT} = \frac{1}{2} \left(1 - \frac{\sum_{k=1}^{N} n_{k,ref}^3}{\sum_{k=1}^{N} n_{k,ref}^2} \right). \tag{25}$$

In conclusion, $m_{0,OPT}$ is independent of the load parameters if $N = 3$ or if all the subspace inductances are equal.

D. EXPRESSION OF $m_{0,opt}$ AS A FUNCTION OF THE DIMENSIONLESS VOLTAGE VECTORS

After tedious calculations, a new form for (22) can be found using (4):

$$m_{0,OPT} = \frac{1}{2} \left(1 - \frac{\sum_{\rho,\sigma,\tau=1,3,\dots}^{N-2} \frac{1}{L_\rho^2} \Re e\{\bar{f}(\rho,\sigma,\tau)\}}{2 \sum_{\rho=1,3,\dots}^{N-2} \frac{1}{L_\rho^2} |\bar{m}_{\rho,ref}|^2} \right). \tag{26}$$

In (26), $\bar{f}$ is a complex function defined as follows:

$$\begin{aligned} \bar{f}(\rho,\sigma,\tau) = {} & \bar{m}_{\rho,ref} \bar{m}_{\sigma,ref} \bar{m}_{\tau,ref} \delta(\rho+\sigma+\tau) \\ & + \bar{m}^*_{\rho,ref} \bar{m}_{\sigma,ref} \bar{m}_{\tau,ref} \delta(-\rho+\sigma+\tau) \\ & + \bar{m}_{\rho,ref} \bar{m}^*_{\sigma,ref} \bar{m}_{\tau,ref} \delta(\rho-\sigma+\tau) \\ & + \bar{m}_{\rho,ref} \bar{m}_{\sigma,ref} \bar{m}^*_{\tau,ref} \delta(\rho+\sigma-\tau) \end{aligned} \tag{27}$$

where "$*$" is the complex conjugate operator, and the binary operator δ is 1 only if its operand is a multiple of N:

$$\delta(n) = \begin{cases} 1, & \text{if } n \bmod N = 0, \\ 0, & \text{otherwise.} \end{cases} \tag{28}$$

The expression of $m_{0,OPT}$ resulting from (26) for three-phase inverters ($N = 3$) is independent of the load inductance:

$$m_{0,OPT}^{(3)} = \frac{1}{2} \left(1 - \frac{\Re e\{\bar{m}_{1,ref}^3\}}{2|\bar{m}_{1,ref}|^2} \right). \tag{29}$$

If $\bar{m}_{1,ref}$ is written in polar form as $M_1 e^{j\theta}$, (29) becomes as follows:

$$m_{0,OPT}^{(3)} = \frac{1}{2} - \frac{1}{4} M_1 \cos 3\theta. \tag{30}$$

This result was originally presented by S. R. Bowes in 1985 [23] and has been known for approximately 40 years.

The expression of $m_{0,OPT}$ for the case $N = 5$ is as follows:

$$m_{0,OPT}^{(5)} = \frac{1}{2} \left[1 - \frac{\Re e\{\bar{f}_1^{(5)} + \bar{f}_2^{(5)}\}}{2\left(\frac{|\bar{m}_{1,ref}|^2}{L_1^2} + \frac{|\bar{m}_{3,ref}|^2}{L_3^2}\right)} \right] \tag{31}$$

where the functions $\bar{f}_1^{(5)}$ and $\bar{f}_2^{(5)}$ are defined below:

$$\begin{aligned} \bar{f}_1^{(5)} &= \bar{m}_{1,ref}^2 \bar{m}_{3,ref} \left(\frac{2}{L_1^2} + \frac{1}{L_3^2} \right) \\ \bar{f}_2^{(5)} &= \bar{m}^*_{1,ref} \bar{m}_{3,ref}^2 \left(\frac{1}{L_1^2} + \frac{2}{L_3^2} \right). \end{aligned} \tag{32}$$

This result aligns with the findings presented in a paper by Casadei et al. in 2011 [28], where $m_{0,OPT}$ was obtained through complex analytical calculations.

Finally, the expression of $m_{0,OPT}$ for the cases $N = 7$ is as follows:

$$m_{0,OPT}^{(7)} = \frac{1}{2} \left[1 - \frac{\Re e\{\bar{f}_1^{(7)} + \bar{f}_2^{(7)} + \bar{f}_3^{(7)} + \bar{f}_4^{(7)}\}}{2\left(\frac{|\bar{m}_{1,ref}|^2}{L_1^2} + \frac{|\bar{m}_{3,ref}|^2}{L_3^2} + \frac{|\bar{m}_{5,ref}|^2}{L_5^2}\right)} \right] \tag{33}$$

where the functions $\bar{f}_1^{(7)}, \bar{f}_2^{(7)}, \dots, \bar{f}_4^{(7)}$ are defined hereafter:

$$\begin{aligned} \bar{f}_1^{(7)} &= \bar{m}_{1,ref} \bar{m}_{3,ref}^2 \left(\frac{1}{L_1^2} + \frac{2}{L_3^2} \right) \\ \bar{f}_2^{(7)} &= \bar{m}_{1,ref}^2 \bar{m}_{5,ref} \left(\frac{2}{L_1^2} + \frac{1}{L_5^2} \right) \\ \bar{f}_3^{(7)} &= \bar{m}^*_{3,ref} \bar{m}_{5,ref}^2 \left(\frac{1}{L_3^2} + \frac{2}{L_5^2} \right) \\ \bar{f}_4^{(7)} &= \bar{m}^*_{1,ref} \bar{m}_{3,ref} \bar{m}_{5,ref} \left(\frac{2}{L_1^2} + \frac{2}{L_3^2} + \frac{2}{L_5^2} \right). \end{aligned} \tag{34}$$

The previous results unequivocally demonstrate that SPWM, which maintains $m_{0,ref}$ equal to 1/2, provides the

minimum ripple of the output currents in multiphase machines whenever only one harmonic sub-space is excited.

III. SIMULATION RESULTS

A. GENERAL RESULTS

A series of numerical simulations was conducted to assess the effectiveness of the developed strategy in comparison with SPWM and SVPWM, which are commonly used when a low output current ripple is desired. Two multi-phase induction machine models with five and seven phases, respectively, were developed in Matlab/Simulink to emulate the behavior of the prototypes utilized in the experimental tests. The parameters of the five-phase machine are presented in Tab. 3, while those of the seven-phase machine are reported in Tab. 4.

The inductance L_ρ that limits the current ripple in subspace ρ is approximately equal to the leakage inductance, which can be calculated as follows:

$$L_\rho = L_{S\rho} - \frac{L_{M\rho}^2}{L_{R\rho}}. \tag{35}$$

The numerical simulations assume that both machines operate in a steady state. Each dimensionless voltage space vector $\bar{m}_{\rho,ref}$ rotates with a constant angular frequency $\rho\omega_1$ and constant magnitude M_ρ, as follows:

$$\bar{m}_{\rho,ref} = M_\rho e^{j\rho\omega_1 t}. \tag{36}$$

where ω_1 is the fundamental frequency of the output voltage.

TABLE 3. Parameters of the five-phase wound-rotor induction machine.

Rated power	$3.5\ kW$
Rated speed	$1500\ RPM$
Pole number	6
Self inductances	$L_{S1} = 0.411\ H, L_{R1} = 0.939\ H$ $L_{S3} = 0.068\ H, L_{R3} = 0.158\ H$
Mutual inductances	$L_{M1} = 0.555\ H$ $L_{M3} = 0.053\ H$
Stator resistances	$R_{S1} = R_{S3} = 1.7\ \Omega$
Rotor resistances	$R_{R1} = R_{R3} = 2.03\ \Omega$

TABLE 4. Parameters of the seven-phase induction machine.

Rated power	$3.5\ kW$
Rated speed	$1450\ RPM$
Pole number	4
Self inductances	$L_{S1}, L_{R1} = 0.1798\ H$ $L_{S3}, L_{R3} = 0.0244\ H$ $L_{S5}, L_{R5} = 0.0120\ H$
Mutual inductances	$L_{M1} = 0.1748\ H$ $L_{M3} = 0.0194\ H$ $L_{M5} = 0.070\ H$
Stator resistances	$R_{S1} = R_{S3} = R_{S5} = 1.1\ \Omega$
Rotor resistances	$R_{R1} = 1.01\ \Omega$ $R_{R3} = 0.8\ \Omega$ $R_{R5} = 0.6\ \Omega$

The average RMS value of the current ripple is calculated over a fundamental period $\frac{2\pi}{\omega_1}$ resulting from the contributions of all the switching periods.

$$\Delta I_{RMS,avg}^2 = \frac{\omega_1}{2\pi}\int_0^{\frac{2\pi}{\omega_1}} \Delta I_{RMS}^2 dt \tag{37}$$

Equation (37) is calculated for all points of the linear-modulation domain [32], [33].

The optimal modulation, SVPWM and SPWM have been compared for the five-phase and seven-phase inverters for three different switching frequencies (3, 5 and 8 kHz) in a range of operational scenarios. The simulation results are presented in tabular form. Tabs. 5 and 6 report the values of the modulation indexes, the RMS value squared of the current ripple for all strategies, and the ratio squared of the RMS value of the current ripple for SVPWM or SPWM over the RMS value of the current ripple for the optimal modulation. In all simulations, these ratios are greater than or equal to 1, indicating that the optimal modulation generates the best current quality.

Numerical simulations have been conducted to replicate the experimental results as closely as possible.

- In some instances, the modulation index is nearly, but not precisely, equal to the maximum value (e.g., 0.47 instead of 0.5). This discrepancy arises due to two factors. First, the inverter dead times preclude the theoretical limit from being reached without introducing distortions in the voltage due to transient overmodulation conditions. The second reason is related to potential fluctuations in the output voltage. As the control system assigns the reference output voltage depending on the operating conditions and the input DC-link voltage, the modulation index may exhibit slight fluctuations. A small margin ensures that the inverter does not enter the overmodulation region, which would cause distortions not considered in the presented theory, which focuses on the linear modulation region.
- Tabs. 5 and 6 demonstrate that, as the switching frequency increases, the optimal strategy remains the most effective, yet the ripple tends to decrease in inverse proportion to the switching frequency. In the experimental tests, the increase in switching frequency may potentially introduce spurious phenomena, such as inverter dead times and core losses, which could affect the measurement accuracy. To mitigate these issues, a frequency of 3 kHz is employed in the experimental tests.

Consequently, the analysis of the simulation results continues in Sections III-B and III-C, respectively, with reference only to the switching frequency of 3 kHz.

B. FIVE-PHASE INVERTER

Fig. 4(a) shows the ratio of the RMS values of the current ripple with SVPWM and the optimal modulation resulting from Tab. 5 when the switching frequency is 3 kHz (blue columns). This quantity is always greater than 1, meaning

TABLE 5. Simulation results for the five-phase induction motor for three different switching frequencies.

Five-phase inverter																
Test	M_1	M_3	$\Delta\bar{I}^2_{RMS,avg,OPT}$			$\Delta\bar{I}^2_{RMS,avg,SPWM}$			$\Delta\bar{I}^2_{RMS,avg,SVPWM}$			$\frac{\Delta\bar{I}^2_{RMS,avg,SPWM}}{\Delta\bar{I}^2_{RMS,avg,OPT}}$			$\frac{\Delta\bar{I}^2_{RMS,avg,SVPWM}}{\Delta\bar{I}^2_{RMS,avg,OPT}}$		
			3 kHz	5 kHz	8 kHz	3 kHz	5 kHz	8 kHz	3 kHz	5 kHz	8 kHz	3 kHz	5 kHz	8 kHz	3 kHz	5 kHz	8 kHz
P_1	0.47	0	0.0439	0.0369	0.0266	0.0439	0.0360	0.0266	0.0449	0.0374	0.0270	1	1	1	1.0227	1.0129	1.0167
P_3	0	0.47	0.0442	0.0370	0.0268	0.0442	0.0370	0.0268	0.0456	0.0374	0.0272	1	1	1	1.0235	1.0124	1.0162
P_{13}	0.32	0.17	0.0374	0.0323	0.0232	0.0426	0.0375	0.0272	0.0384	0.0328	0.0239	1.1410	1.1615	1.1818	1.0288	1.0149	1.057

TABLE 6. Simulation results for the seven-phase induction motor for three different switching frequencies.

Seven-phase inverter																	
Test	M_1	M_3	M_5	$\Delta\bar{I}^2_{RMS,avg,OPT}$			$\Delta\bar{I}^2_{RMS,avg,SPWM}$			$\Delta\bar{I}^2_{RMS,avg,SVPWM}$			$\frac{\Delta\bar{I}^2_{RMS,avg,SPWM}}{\Delta\bar{I}^2_{RMS,avg,OPT}}$			$\frac{\Delta\bar{I}^2_{RMS,avg,SVPWM}}{\Delta\bar{I}^2_{RMS,avg,OPT}}$		
				3 kHz	5 kHz	8 kHz	3 kHz	5 kHz	8 kHz	3 kHz	5 kHz	8 kHz	3 kHz	5 kHz	8 kHz	3 kHz	5 kHz	8 kHz
P_1	0.3	0	0	0.04001	0.0240	0.0163	0.04001	0.0240	0.01630	0.0399	0.02410	0.01641	1	1	1	1.0098	1.0036	1.0019
P_{13}	0.1	0.25	0	0.03756	0.02281	0.0155	0.03789	0.02341	0.01610	0.03763	0.02275	0.0156	1.0091	1.0263	1.0358	1.0019	1.0015	1.0031
P_{15}	0.27	0	0.12	0.03855	0.02341	0.01650	0.04029	0.02490	0.0173	0.03861	0.02347	0.01654	1.0452	1.0641	1.0502	1.0017	1.0029	1.0052
P_{135}	0.15	0.15	0.12	0.03143	0.02030	0.0140	0.03664	0.02379	0.0170	0.03146	0.02381	0.0141	1.1671	1.1724	1.2164	1.0012	1.0014	1.0062
P_{35}	0	0.15	0.15	0.03332	0.01951	0.01318	0.03357	0.01989	0.01349	0.03342	0.01958	0.01319	1.0078	1.0191	1.0237	1.0031	1.0032	1.0008

the current ripple generated by the optimal strategy is lower. In particular, the proposed strategy performs better in two regions, i.e., for values of M_3 around 0.525, and when M_1 is slightly greater than M_3. In the latter situation, SVPWM generates a higher current ripple than the optimal strategy by 4.5%. When M_1 is close to 0.525, the current ripple is the same for both strategies.

Fig. 4(b) compares the current ripples resulting from SPWM and the optimal modulation. SPWM generates a current ripple that is 25% higher when M_1 and M_3 tend to coincide.

Fig. 5 shows that the optimal strategy is more efficient than SVPWM near the boundary of the linear modulation region. Compared to the optimal modulation, SVPWM causes a number of commutations (N_{sw}) that can be 25% greater when M_1 and M_3 are close to the domain boundary. This result is due to a decrease in the number of commutations of the optimal strategy when $m_{0,OPT}$ is saturated by the lower bound $m_{0,DMIN}$ or the upper bound $m_{0,DMAX}$.

Fig. 6 illustrates this phenomenon. The waveform of $m_{0,OPT}$ is shown when M_1 is 0.4, M_3 is 0.2. It turns out that $m_{0,OPT}$ becomes alternately equal to $m_{0,DMAX}$ or $m_{0,DMIN}$, so only four legs of the inverter out of five do switch.

Conversely, SPWM and the optimal modulation exhibit the same number of commutations in the shared part of the linear modulation range. However, the achievable voltage range of the optimal modulation is wider and is equal to that of SVPWM [32], [33].

C. SEVEN-PHASE INVERTER

The 3D plots in Figs. 7a and 7b show the ratio of the RMS value of the current ripple caused by SVPWM or SPWM and the optimal modulation for a seven-phase induction motor drive resulting from Tab. 6 when the switching frequency is 3 kHz (blue columns). The representation is semi-transparent and qualitatively depicts the behavior of the optimal modulation strategy within the linear modulation domain. Fig. 7(a) shows that the RMS value of the current ripple generated by SVPWM is up to 2% higher than that of the optimal strategy in the center of the linear modulation region ($M_1 \simeq M_3 \simeq M_5$)

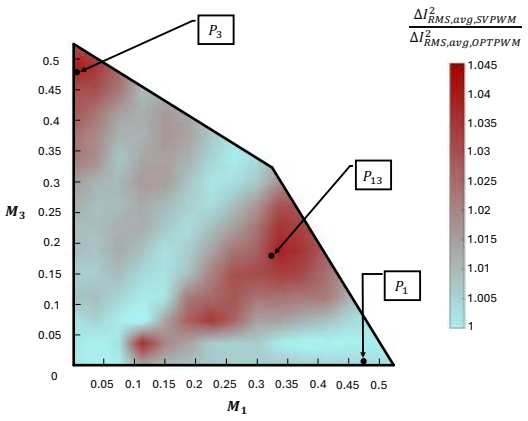

(a)

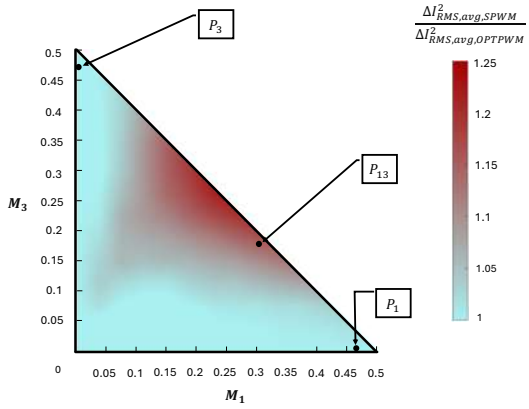

(b)

FIGURE 4. Performance of the optimal modulation in a five-phase inverter. a) Ratio between the RMS value of the current ripple with SVPWM and the optimal modulation. b) Ratio between the RMS value of the current ripple with SPWM and the optimal modulation.

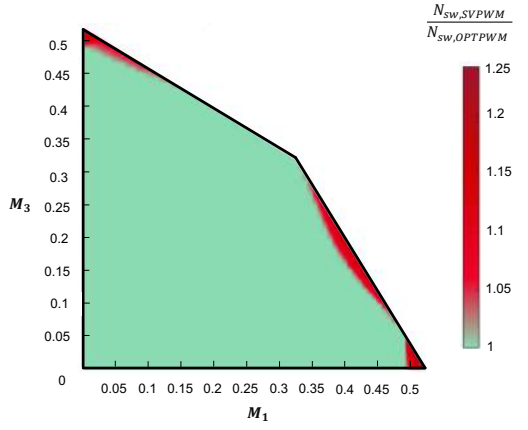

FIGURE 5. Ratio among the numbers of commutations obtained with SVPWM and the optimal modulation for a five-phase inverter.

or when one of the three dimensionless voltages is near zero.

Fig. 7(b) shows a similar behavior for SPWM. Compared to the optimal strategy, SPWM generates a current ripple that

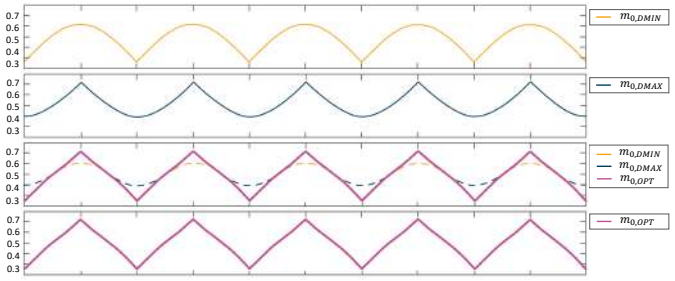

FIGURE 6. Waveform of $m_{0,OPT}$ clamped to $m_{0,DMIN}$ or $m_{0,DMAX}$ for $M_1 = 0.4$ and $M_3 = 0.2$. The horizontal scale for ωt is 36°/div.

is 25% higher when M_1, M_3, and M_5 are in close proximity to one another or when one of them is zero and the other ones tend to coincide.

Finally, it is noteworthy that the proposed method reduces the number of commutations by up to 14% compared to SVPWM when $M_1 \simeq M_3 \simeq M_5$ and at some points on the boundary close to the overmodulation region as shown in Fig. 8. Conversely, the optimal modulation and SPWM have the same number of commutations in the shared part of the voltage range. However, the SPWM voltage range is smaller.

IV. EXPERIMENTAL RESULTS

Some experimental tests were carried out to validate the theoretical analysis. Fig. 9 depicts the entire experimental setup, including the five- and seven-phase induction machines. A DC generator operates as a load mechanically coupled to the machines. The machine parameters are the same as those used for the simulation results and reported in Tabs. 3 and 4. The control system is developed through a dSPACE MicroLabBox platform, which controls a multiphase inverter with a switching frequency of 3 kHz, configured to supply a multiphase motor with a maximum of twelve phases. The inverter power stage consists of two Infineon F12-25R12KT4G power modules, equipped with 1200 V – 25 A class IGBTs and diodes. An Elektro-Automatik power supply (EA-PS 9500 - 20) keeps the DC-link voltage at about 200 V and 250 V respectively for the five- and seven-phase configurations.

The current ripple is approximately inversely proportional to the switching frequency and machine high-frequency inductance. However, the machine parameters are contingent upon the specific switching frequency, machine type, and rotor slots. Furthermore, as the frequency varies, other phenomena may occur, which are caused by losses in the machine iron core due to eddy currents and hysteresis (loss phenomena in machines with surface PMs can also occur as a result of induced currents within the magnets). These problems are intricate and complex to address. The use of a constant frequency of 3 kHz in experimental tests has been dictated by these factors:

- The duration of the switching period should be sufficiently long to allow for accurate measurement of the

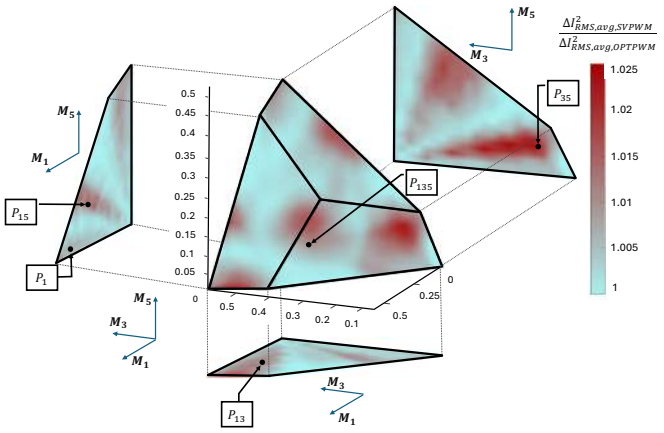

(a)

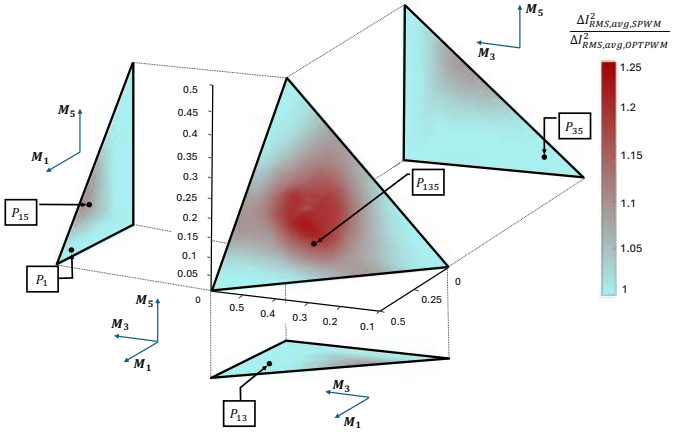

(b)

FIGURE 7. **Performance of the optimal modulation in a seven-phase inverter. Ratio of the RMS values of the current ripple due to SVPWM (a) or SPWM (b) and the optimal modulation.**

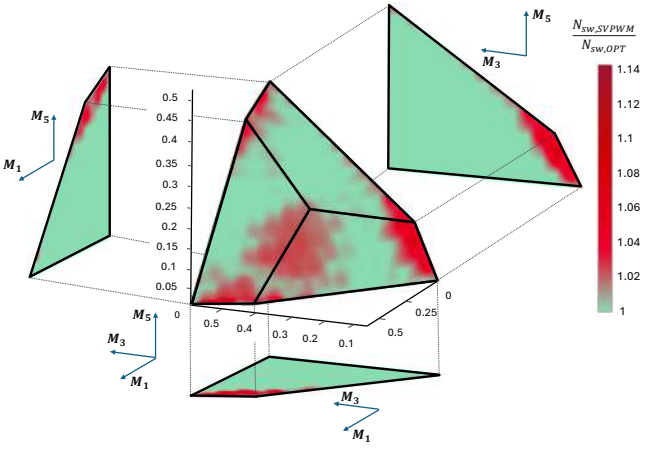

FIGURE 8. **Ratio of the numbers of commutations due to SVPWM and the optimal strategy for a seven-phase inverter.**

current ripple and to minimize the impact of the inverter dead times.

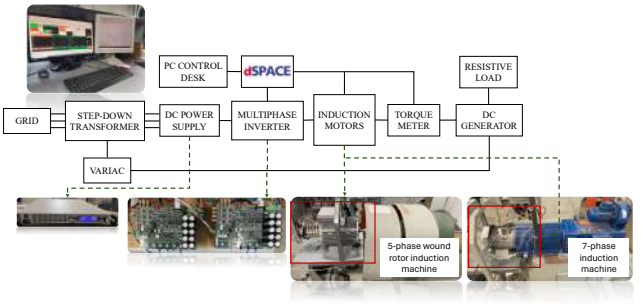

FIGURE 9. **Experimental setup.**

- Simultaneously, the switching period should not be too long since this would result in the linearization approximation of the equations becoming invalid.
- The impact of high-frequency losses on parasitic phenomena should be negligible.

The use of induction machines for the experimental tests is not accidental. In PM machines, permanent magnets generate high-order harmonic back-electromotive forces that result in the circulation of harmonic currents. These components typically operate at a frequency that is much lower than the switching frequency and do not affect the high-frequency current ripple. However, the control system must compensate for them in order to track the current reference. This control action interferes with the experimental tests and the calculation of the modulation index.

A. FIVE-PHASE INVERTER

The simulation results obtained in Section III-B have been validated through experimental tests. The test conditions correspond to the values of M_1 and M_3 highlighted in Fig. 4. The test results are listed in Tab. 7. At points P_1 and P_3, either M_1 or M_3 is zero. In accordance with the theory developed in Section II-D, $m_{0,ref}$ equals 1/2 in both cases, and the optimal modulation coincides with the SPWM. As expected, the current ripple of SVPWM is slightly higher. At point P_{13}, the current ripple due to SPWM and SVPWM is greater than that of the optimal modulation, although the expected difference is more significant. Finally, Fig. 10 shows the waveform of the current ripple generated by the optimal modulation when the motor operates at a fundamental frequency of 10 Hz with and without injection of third harmonic currents. Fig. 10(a) presents the operating conditions of point P_1, while Fig. 10(b) refers to the operating conditions of point P_{13}.

Fig. 11 illustrates the spectrum of the phase current when the five-phase machine is operating at point P_{13}. The reference voltage vectors, which rotate at 10 Hz and 30 Hz, generate harmonic components in the phase current at the same frequencies, as can be observed in the detail window displaying the current spectrum up to 40 Hz. The amplitude of the fundamental component is identical for all strategies.

TABLE 7. Performance of the optimal modulation strategy for the five-phase induction machine.

Test	M_1	M_3	$\frac{\Delta I^2_{RMS,avg,SPWM}}{\Delta I^2_{RMS,avg,OPT}}$	$\frac{\Delta I^2_{RMS,avg,SVPWM}}{\Delta I^2_{RMS,avg,OPT}}$
P_1	0.47	0	1	1.0116
P_3	0	0.47	1	1.0206
P_{13}	0.32	0.17	1.1248	1.0265

Similarly, the third harmonic component of the phase current is independent of the strategy employed, thereby confirming that the reference voltage vectors are identical for all strategies. As can be observed in the second detail window, the spectrum around 3 kHz exhibits modulation sidebands situated at approximately the switching frequency. The spectral density of the optimal modulation is demonstrably lower than that of the other strategies.

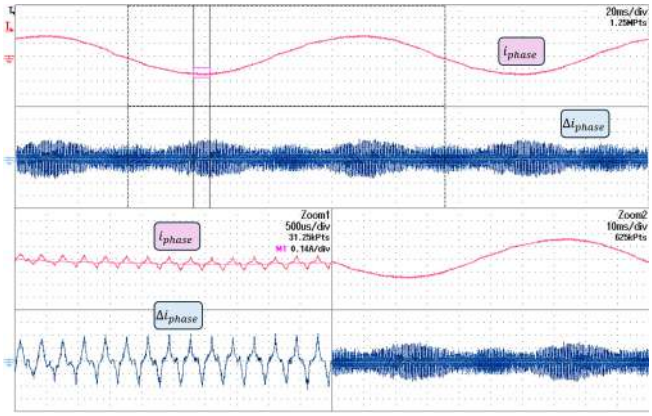

(a)

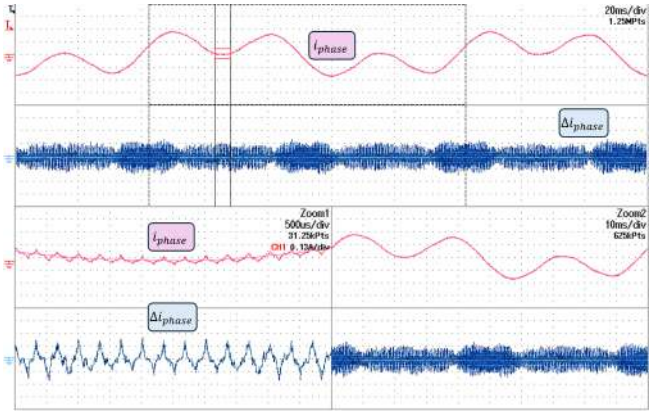

(b)

FIGURE 10. Waveform of the phase current of the five-phase induction machine when the fundamental frequency is 10 Hz. a) Operating point P_1. b) Operating point P_{13}. From top to bottom: phase current (1.34 A/div), phase current ripple $\triangle i$ (0.13 A/div).

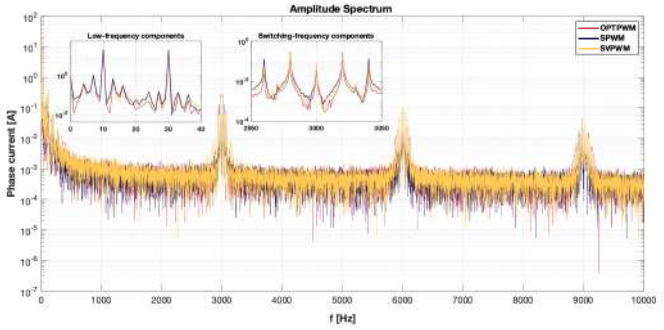

FIGURE 11. Spectrum of the phase current in the operating point P_{13} for the five-phase inverter.

TABLE 8. Performance of the optimal modulation strategy for the seven-phase induction machine.

Test	M_1	M_3	M_5	$\frac{\Delta I^2_{RMS,avg,SPWM}}{\Delta I^2_{RMS,avg,OPT}}$	$\frac{\Delta I^2_{RMS,avg,SVPWM}}{\Delta I^2_{RMS,avg,OPT}}$
P_1	0.3	0	0	1	1.001
P_{13}	0.1	0.25	0	1.008	1.0013
P_{15}	0.27	0	0.12	1.0359	1.0018
P_{135}	0.15	0.15	0.12	1.1503	1.0146
P_{35}	0	0.15	0.15	1.005	1.021

B. SEVEN-PHASE INVERTER

Some experimental tests were performed to verify the results presented in Section III-C. The test points are highlighted in Fig. 7, and the experimental results are reported in Tab. 8. In accordance with the theoretical predictions, the optimal strategy outperforms SVPWM at all points. Similarly, the RMS value of the current ripple due to SPWM is greater than that of the optimal modulation by up to 15%, except for points where the two strategies coincide, such as P_1 and P_3. Finally, Fig. 12 shows the waveform of the current ripple generated by the optimal modulation when the motor operates at a fundamental frequency of 10 Hz with and without injection of third harmonic currents. Fig. 12(a) shows the operating conditions at point P_1, while Fig. 12(b) shows the operating conditions at point P_{135}.

Fig. 13 illustrates the spectrum of the phase current when the seven-phase machine operates at point P_{135}. The reference voltage vectors rotate at 10 Hz, 30 Hz, and 50 Hz, thereby generating the corresponding current harmonic components, as can be observed in the detail window displaying the current spectrum up to 70 Hz. All strategies result in the same amplitude for the fundamental, third, and fifth harmonic components. Once more, the spectrum in the vicinity of 3 kHz, as displayed in the second detail window, exhibits modulation sidebands around the switching frequency. The lowest spectral density is that of the optimal modulation.

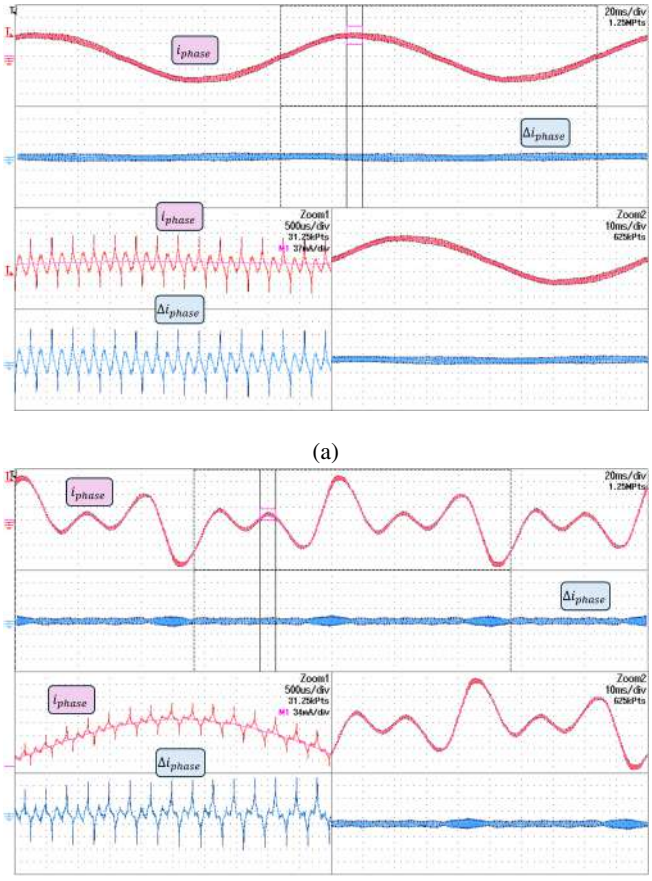

FIGURE 12. **Waveform of the phase current of the seven-phase induction machine when the fundamental frequency is 10 Hz. a) Operating point P_1. b) Operating point P_{135}. From top to bottom: phase current (0.25 A/div), phase current ripple $\triangle i$ (0.035 A/div).**

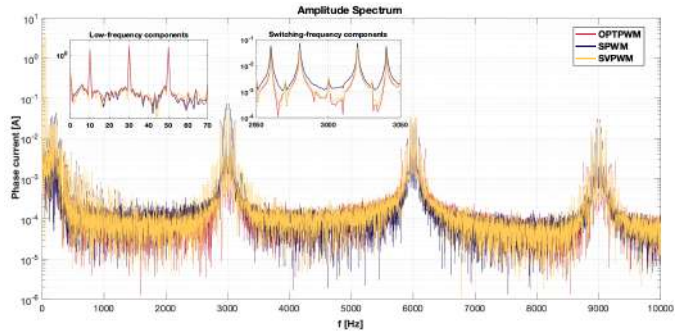

FIGURE 13. **Spectrum of the phase current in the operating point P_{135} for the seven-phase inverter.**

V. CONCLUSION

This paper presents a theoretical analysis to minimize the RMS value of the load current ripple in multiphase inverters with any odd number of phases. The developed approach provides a closed-form solution for the optimal zero-sequence component of the modulating signals, which is a function of the reference voltages or desired voltage vectors and the load high-frequency equivalent inductances. Therefore, this strategy is not limited to sinusoidal signals or steady-state conditions. On average, the proposed approach may theoretically reduce the RMS value of the load current ripple by up to 4% for five-phase inverters and 2% for seven-phase inverters compared to the SVPWM technique. When compared to SPWM, the reduction can be up to 25%, depending on the operating conditions. Moreover, the proposed technique reduces the number of switch commutations when high reference voltages are required, i.e., for values of the modulating indices close to the overmodulation region. The reduction may be up to 25% for five-phase inverters and 15% for seven-phase inverters. Consequently, power electronic switches experience a reduction in switching losses. The experimental results have confirmed the trends expected by the theoretical analysis. Although some of these findings have already been reported in the literature in special cases, this study provides a coherent theoretical motivation. The theoretical results were validated by numerical and experimental tests with five- and seven-phase induction motors.

REFERENCES

[1] F. Barrero and M. J. Duran, "Recent advances in the design, modeling, and control of multiphase machines—part i," *IEEE Trans. on Ind. Elect.*, vol. 63, no. 1, pp. 449–458, 2016.

[2] M. J. Duran and F. Barrero, "Recent advances in the design, modeling, and control of multiphase machines—part ii," *IEEE Trans. on Ind. Elect.*, vol. 63, no. 1, pp. 459–468, 2016.

[3] W. Taha, P. Azer, A. D. Callegaro, and A. Emadi, "Multiphase traction inverters: State-of-the-art review and future trends," *IEEE Access*, vol. 10, pp. 4580–4599, 2022.

[4] E. Levi, "Advances in converter control and innovative exploitation of additional degrees of freedom for multiphase machines," *IEEE Trans. on Ind. Elect.*, vol. 63, no. 1, pp. 433–448, 2016.

[5] A. Lega, M. Mengoni, G. Serra, A. Tani, and L. Zarri, "Space vector modulation for multiphase inverters based on a space partitioning algorithm," *IEEE Trans. on Ind. Elect.*, vol. 56, no. 10, pp. 4119–4131, 2009.

[6] O. López, J. Álvarez, A. G. Yepes, F. Baneira, D. Pérez-Estévez, F. D. Freijedo, and J. Doval-Gandoy, "Carrier-based pwm equivalent to multilevel multiphase space vector pwm techniques," *IEEE Trans. on Ind. Elect.*, vol. 67, no. 7, pp. 5220–5231, 2020.

[7] B. Yu, W. Song, and Y. Guo, "A simplified and generalized svpwm scheme for two-level multiphase inverters with common-mode voltage reduction," *IEEE Trans. on Ind. Elect.*, vol. 69, no. 2, pp. 1378–1388, 2022.

[8] A. Chakrabarti, K. Sarkar, P. R. Kasari, B. Das, and S. K. Biswas, "A cb-pwm technique for eliminating cmv in multilevel multiphase vsi," *IEEE Trans. on Ind. Elect.*, vol. 70, no. 9, pp. 8666–8675, 2023.

[9] L. Zarri, M. Mengoni, A. Tani, G. Serra, and D. Casadei, "Minimization of the power losses in igbt multiphase inverters with carrier-based pulsewidth modulation," *IEEE Trans. on Ind. Elect.*, vol. 57, no. 11, pp. 3695–3706, 2010.

[10] L. Vancini, M. Mengoni, G. Rizzoli, G. Sala, L. Zarri, and A. Tani, "Carrier-based pwm overmodulation strategies for five-phase inverters," *IEEE Tran. on Pow. Elect.*, vol. 36, no. 6, pp. 6988–6999, 2021.

[11] A. G. Yepes and J. Doval-Gandoy, "Overmodulation method with adaptive *x*-*y* current limitation for five-phase induction motor drives," *IEEE Trans. on Ind. Elect.*, vol. 69, no. 3, pp. 2240–2251, 2022.

[12] L. Aarniovuori, P. Rasilo, M. Niemelä, and J. J. Pyrhönen, "Analysis of 37-kw converter-fed induction motor losses," *IEEE Trans. on Ind. Elect.*, vol. 63, no. 9, pp. 5357–5365, 2016.

[13] R. Kumar and P. Kumar, "Core loss estimation for an inverter-fed induction motor with more accurate realisation of material non-linearity and impact of hysteresis minor loops," *IEEE Trans. on En. Conv.*, vol. 37, no. 1, pp. 327–336, 2022.

[14] G. K. Sakkas and A. G. Kladas, "Particular model for efficient switching frequency loss consideration in surface mounted permanent magnets," *IEEE Trans. on Mag.*, vol. 59, no. 5, pp. 1–5, 2023.
[15] I. Sirotić, M. Kovačić, and S. Stipetić, "Methodology and measurement setup for determining pwm contribution to iron loss in laminated ferromagnetic materials," *IEEE Trans. on Ind. App.*, vol. 57, no. 5, pp. 4796–4804, 2021.
[16] L. Chang, M. Alvi, W. Lee, J. Kim, and T. M. Jahns, "Efficiency optimization of pwm-induced power losses in traction drive systems with ipm machines using wide bandgap-based inverters," *IEEE Trans. on Ind. App.*, vol. 58, no. 5, pp. 5635–5649, 2022.
[17] A. Edpuganti and A. K. Rathore, "A survey of low switching frequency modulation techniques for medium-voltage multilevel converters," *IEEE Trans. on Ind. App.*, vol. 51, no. 5, pp. 4212–4228, 2015.
[18] G. Liang, W. Liao, Z. Zhang, D. Ni, S. Huang, M. Li, Y. Wen, and J. Gao, "An optimized pulsewidth modulation for dual three-phase pmsm under low carrier ratio," *IEEE Trans. on Pow. Elect.*, vol. 37, no. 3, pp. 3062–3072, 2022.
[19] M. Gu, Z. Wang, P. Liu, and J. He, "Comparative study of advanced modulation and control schemes for dual three-phase pmsm drives with low switching frequencies," *IEEE Trans. on Trans. Elect.*, vol. 10, no. 1, pp. 962–975, 2024.
[20] H.-S. Jung, C.-E. Hwang, H.-S. Kim, S.-K. Sul, A. Hee-Won, and H. Yoo, "Minimum torque ripple pulse width modulation with reduced switching frequency for medium-voltage motor drive," *IEEE Trans. on Ind. App.*, vol. 54, no. 4, pp. 3315–3325, 2018.
[21] X. Wang, H. Yan, G. Sala, G. Buticchi, C. Gu, W. Zhao, L. Xu, and H. Zhang, "Selective torque harmonic elimination for dual three-phase pmsms based on pwm carrier phase shift," *IEEE Trans. on Pow. Elect.*, vol. 35, no. 12, pp. 13 255–13 269, 2020.
[22] X. Zhang, T. Yang, and S. Bozhko, "Speed/torque ripple reduction of high-speed permanent magnet starters/generators with low inductance for more electric aircraft applications," *IEEE Trans. on Trans. Elect.*, vol. 8, no. 4, pp. 4431–4443, 2022.
[23] A. M. S. R. Bowes, "Suboptimal switching strategies for micropocessor-controlled pwm inverter drives," *IEE Proceedings*, vol. 132, no. 3, pp. 133–148, 1985.
[24] D. Dujic, M. Jones, and E. Levi, "Analysis of output current ripple rms in multiphase drives using space vector approach," *IEEE Trans. on Ind. Elect.*, vol. 24, no. 8, pp. 1926–1938, 2009.
[25] ——, "Analysis of output current-ripple rms in multiphase drives using polygon approach," *IEEE Trans. on Pow. Elect.*, vol. 25, no. 7, pp. 1838–1849, 2010.
[26] D. Dujic, M. Jones, E. Levi, J. Prieto, and F. Barrero, "Switching ripple characteristics of space vector pwm schemes for five-phase two-level voltage source inverters—part 1: Flux harmonic distortion factors," *IEEE Trans. on Ind. Elect.*, vol. 58, no. 7, pp. 2789–2798, 2011.
[27] M. Jones, D. Dujic, E. Levi, J. Prieto, and F. Barrero, "Switching ripple characteristics of space vector pwm schemes for five-phase two-level voltage source inverters—part 2: Current ripple," *IEEE Trans. on Ind. Elect.*, vol. 58, no. 7, pp. 2799–2808, 2011.
[28] D. Casadei, M. Mengoni, G. Serra, A. Tani, and L. Zarri, "A new carrier-based pwm strategy with minimum output current ripple for five-phase inverters," in *Proc. of EPE 2011*, 2011, pp. 1–10.
[29] G. Grandi and J. Loncarski, "Evaluation of current ripple amplitude in five-phase pwm voltage source inverters," in *Eurocon 2013*, 2013, pp. 1073–1080.
[30] D. Glose and R. Kennel, "Carrier-based pulse width modulation for symmetrical six-phase drives," *IEEE Trans. on Pow. Elect.*, vol. 30, no. 12, pp. 6873–6882, 2015.
[31] S. Paul and K. Basu, "Linear pwm techniques of asymmetrical six-phase machine with optimal current ripple performance," *IEEE Trans. on Ind. Elect.*, vol. 70, no. 2, pp. 1298–1309, 2023.
[32] D. Casadei, D. Dujic, E. Levi, G. Serra, A. Tani, and L. Zarri, "General modulation strategy for seven-phase inverters with independent control of multiple voltage space vectors," *IEEE Trans. on Ind. Elect.*, vol. 55, no. 5, pp. 1921–1932, 2008.
[33] E. Levi, D. Dujic, M. Jones, and G. Grandi, "Analytical determination of dc-bus utilization limits in multiphase vsi supplied ac drives," *IEEE Trans. on En. Conv.*, vol. 23, no. 2, pp. 433–443, 2008.

ANTONIO FEMIA received the M.Sc. degree, with honors, in Electrical Engineering from the University of Bologna, Bologna, Italy, in 2021. Currently, he is pursuing a PhD in electrical engineering with the Department of Electric, Electronic and Information Engineering "G. Marconi", University of Bologna. His research fields include artificial intelligence applied to electric drives, diagnostic techniques for multiphase machines, and control strategies for power electronic converters.

MICHELE MENGONI (M'13) received the M.S. (with honors) and Ph.D. degrees in electrical engineering from the University of Bologna, Bologna, Italy, in 2006 and 2010, respectively. He is currently an Associate Professor with the Department of Electric, Electronic and Information Engineering "G. Marconi", University of Bologna. His research interests include design, analysis, and control of three phase electric machines, multiphase drives, and ac/ac matrix converters.

LUCA VANCINI received the M.Sc. degree in Electrical Engineering in 2018 from the University of Bologna, Bologna, Italy. Currently he is a postdoctoral fellow with the Department of Electric, Electronic and Information Engineering "G. Marconi", University of Bologna. His research interests include power electronics, control of multiphase converters and diagnostic techniques for multiphase machines.

GABRIELE RIZZOLI received the M.Sc and Ph.D. degree in Electrical Engineering respectively in 2012 and 2016, from the University of Bologna, Bologna, Italy. He is currently an Assistant Professor at the Department of Electrical, Electronic and Information Engineering "G. Marconi" of the University of Bologna. His research interests include the design of electrical machines, the development and control of high-efficient power converters for automotive and renewable energy applications.

LUCA ZARRI (M'05-SM'12) was born in Bologna, Italy. He received the M. Sc. with honors and the Ph.D. degree in Electrical Engineering from the University of Bologna, Bologna, Italy, in 1998 and 2007, respectively. He is currently a Full Professor of power electronics, electric machines and drives with the Department of Electrical, Electronic and Information Engineering "G. Marconi", University of Bologna. He has authored or coauthored more than 170 scientific papers. His research activity concerns the control of power converters and electric drives. He is a senior member of the IEEE Industry Applications, IEEE Power Electronics and IEEE Industrial Electronics Societies. He served as an officer of the IEEE IAS Industrial Drives Committee from 2016 to 2023 and is currently the IAS Industrial Power Conversion Systems Department Vice Chair.

ANGELO TANI was born in Faenza, Italy, in 1963. He received the M. Sc. degree in Electrical Engineering, with honors, from the University of Bologna, Bologna, Italy, in 1988. Currently he is a Full Professor of power electronics, electrical machines and drives with the Department of Electrical, Electronic and Information Engineering "Guglielmo Marconi", University of Bologna. He has authored more than 200 papers published in technical journals and conference proceedings. His current activities include modelling, control and fault diagnosis of multiphase electric machines.